

Wind Tunnel Investigation of the Wind Patterns in the Launching Pad Area of the Brazilian Alcântara Launch Center

Amanda Felipe Faria^{*1}, Ana Cristina Avelar², Gilberto Fisch³

Faria AF  <https://orcid.org/0000-0002-3349-0515>

Avelar AC  <https://orcid.org/0000-0002-0333-4570>

Fisch G  <https://orcid.org/0000-0001-6668-9988>

How to cite

Faria AF; Avelar AC; Fisch G (2019) Wind Tunnel Investigation of the Wind Patterns in the Launching Pad Area of the Brazilian Alcântara Launch Center. *J Aerosp Technol Manag*, 11: e0719. <https://doi.org/10.5028/jatm.v11.996>

ABSTRACT: This paper presents a wind tunnel study of the flow patterns in the main Brazilian Space Port, the Alcântara Launch Center (ALC), located in the Northwest region, over an irregular coastal cliff of 40 m height. In the ALC region, constant winds of strong incidence are very common, which can change the characteristics of the atmospheric boundary layer and affect safety conditions during launching operations. This study was conducted using a scaled model of the Launching Pad Area (LPA) in ALC complex with the purpose of getting insights about the wind flow patterns, as zones of strong vorticity, in that region when the wind incidence angle and coastal cliff characteristics change. The experiments were carried out in an aerodynamic wind tunnel, and for this reason it was necessary to use some techniques described in the literature to simulate an atmospheric boundary layer in a short test section wind tunnel. Hot-wire anemometer measurements were carried out for turbulence level evaluation with empty wind tunnel test section, and a two-dimensional Particle Image Velocimetry (PIV) was used for flow field velocity measurements in different configurations of wind incidence angle (α), Reynolds number and coastal cliff slope angle (β).

KEYWORDS: Alcântara Launch Center (ALC), Particle Image Velocimetry (PIV), Wind incidence, Mobile Integration Tower (MIT), Launching Pad Area (LPA).

INTRODUCTION

Physical phenomena related to wind incidence on buildings are very complex since it is associated to the occurrence of large vortex structures formed from the body shear layer and shed downstream, which distinguishes these flows from those over streamlined bodies (Vatistas *et al.* 1986).

In order to get insights about these complex phenomena, it is necessary to investigate the atmospheric flow features over the related territories. In the case of sounding rockets and satellite launch vehicle, for an effective launching operation, the understanding of environmental conditions is fundamental (Vaughan and Johnson 2011).

Many researches about wind incidence on constructions, or on bluff bodies, can be found in the literature in the latest 50 years, some of them with the purpose of describing the produced wakes, like Woo *et al.* (1977), Griffin (1985), Baskaran and Kashef (1996) and Meneghini *et al.* (2010).

The turbulence in wakes of buildings was investigated with the purpose of guaranteeing the operational safety of aircrafts at airfields, which are very vulnerable to turbulence and quick changes in wind speed. Tests in wind tunnel about buildings of many

1. Departamento de Ciência e Tecnologia Aeroespacial – Instituto Tecnológico de Aeronáutica – Divisão de Aeronáutica – São José dos Campos/SP – Brazil.

2. Departamento de Ciência e Tecnologia Aeroespacial – Instituto de Aeronáutica e Espaço – Divisão de Aerodinâmica – São José dos Campos/SP – Brazil.

3. Departamento de Ciência e Tecnologia Aeroespacial – Instituto de Aeronáutica e Espaço – Divisão de Ciências Atmosféricas – São José dos Campos/SP – Brazil.

*Correspondence author: amanda.felippe.faria@gmail.com

Received: 06 Apr 2017 | Accepted: 08 Apr 2018

Section Editor: João Azevedo



sizes and aspect ratios in a simulated atmospheric boundary layer were carried out, and detailed information on mean longitudinal velocity and turbulence intensity were found.

Wind tunnel measurements have been carried out for studying the flow patterns in the main center of rocket launching in Brazil, the Alcântara Launch Center (ALC), which has some advantages in comparison to others rocket launch in the world due its privileged location (Fig. 1a). It is situated in the Atlantic coast, close to the Equator ($2^{\circ}19' S$; $44^{\circ}22' W$), a privilege shared only with the Guiana Space Center. In addition, a stable climate permits reliability in scheduling the launching operations.

Despite of all positive aspects, ALC has in its topology a coastal cliff of about 40 m high at the edge of the sea land (Fig. 1b), which can modify the atmospheric boundary layer characteristics, and in some conditions may affect safety during launching operations since the rockets launch pad and the Mobile Integration Tower (MIT) (Pires 2009), the building where the space vehicles are assembled and prepared for launching operation, are situated around 150 – 200 m from the sea border, respectively. The MIT has a length of 33 m and a metallic structure.

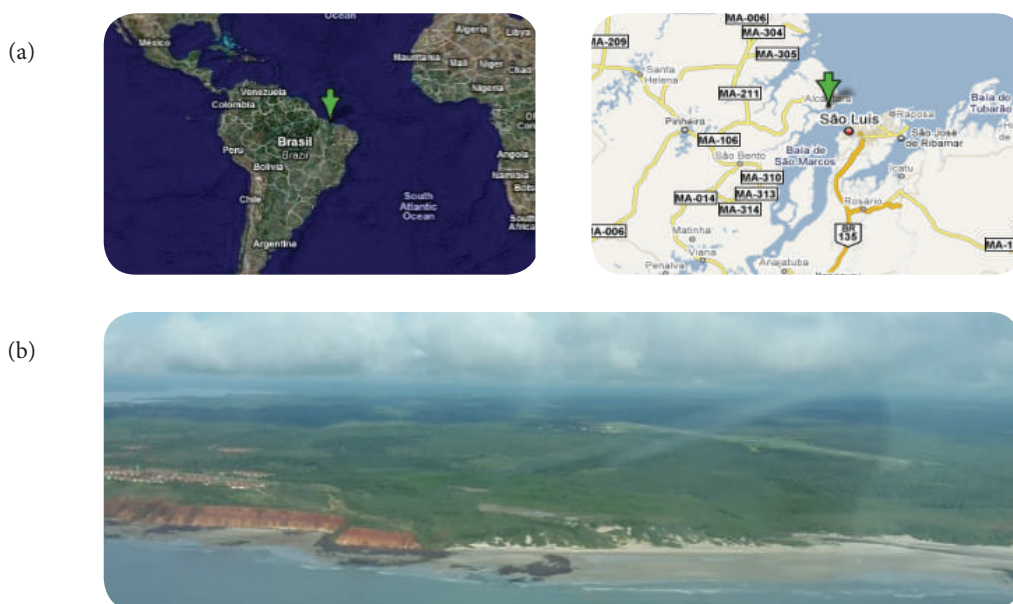


Figure 1. (a) ALC localization; (b) Coastal Cliff at ACL – aerial view.

In the last years, the flow patterns at ALC have been studied by scientists of the *Instituto de Aeronáutica e Espaço* (IAE), in São José dos Campos, sometimes in collaboration with researchers from other institutions, as for example the Federal University of Rio Grande do Sul (Wittwer 2006) and *Instituto Nacional de Pesquisas Espaciais* (INPE) (Pires 2009). The wind characteristics in ALC have already been studied through field measurement (Fisch 1999; Roballo 2007; Marciotto *et al.* 2012), numerical simulations (Pires 2009) and wind tunnel experiments (Pires 2009; Avelar *et al.* 2014).

As a continuation of previous studies about the wind flow patterns in ALC, the emphasis of the present study is the wind flow patterns in the Launch Pad Area (LPA) in a configuration in which the vehicle is inside the MIT (Fig. 2) and the configuration where the launch vehicle is waiting to be launched, positioned 55 m from the MIT and near the exit tower. The exit tower is 24.2 m high and it has a concrete structure that allows the workers to evacuate this building in case of danger.

The bluff bodies do not have an aerodynamic profile, because the flow separates near its border and created vortexes behind the bodies can disturb the flow patterns (Fox *et al.* 2014).

In the present study, a wind tunnel analysis using the technique of Particle Image Velocimetry (PIV) was conducted in order to get more insights about the wind flow patterns in the ALC, more specifically in the LPA region. It was simulated different wind incidence angles (α) considering the main wind incidences directions in ACL and coastal cliff inclination slope (β), for identifying flow regions of strong vorticity and the tri-dimensionality mainly in the neighborhood of the Mobile Integration Tower (MIT).



Figure 2. Launch Pad Area (LPA).

The vortexes pattern behind the MIT or exit tower structures is strongly influenced by the wind incidence angles. These vortexes may induce vibrations or load excess on these buildings structures if they remain there for a long time.

METODOLOGY

ATMOSPHERIC BOUNDARY LAYER

The air flow near the surface is turbulent and the interaction with the air at upper altitude originates the atmospheric boundary layer (ABL). The ABL is defined as a portion of the lower troposphere component, which is influenced by the earth surface, and has forcing with time scale less than hours. These forcing can be: atmospheric dispersion of propellants, heat transfer, drag, friction, evaporation and changes in outflow due to topographic region (Loredo-Souza *et al.* 2004).

The ABL surface can extend from some meters or kilometers, depending of the terrain roughness, wind distance over this surface and thermal atmospheric conditions along the day (Roballo 2007).

The turbulence intensity in the ABL is associated with the mean velocity flow and it has a higher Reynolds number. The turbulent structure of ABL is similar to the two-dimensional boundary layer simulated in a wind tunnel. This similarity is because the ABL structure and boundary layer simulated are formed for two layers: outer layer, more distant from the floor, and inner layer, near the floor. The Fig. 3 shows the estimated height of each layer of the ABL (Loredo-Souza *et al.* 2004; Pires 2009).

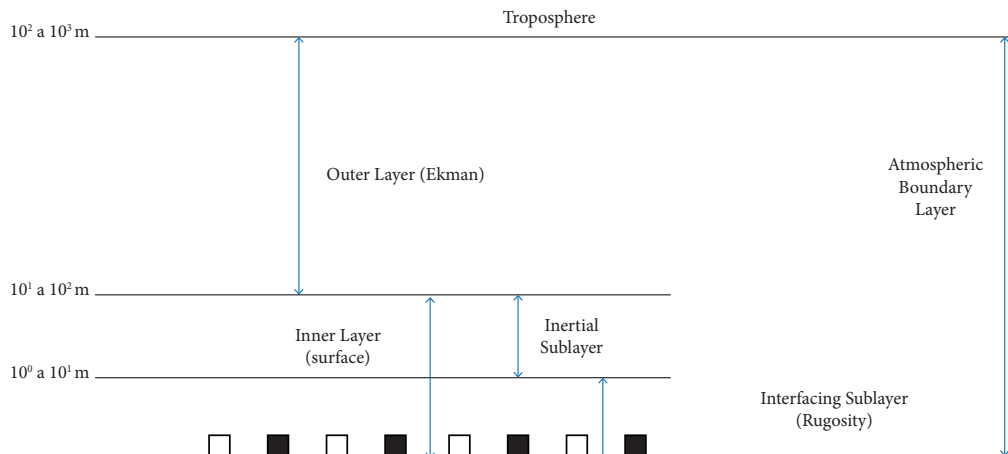


Figure 3. Atmospheric boundary layer structure (Adapted from Garrat 1992).

WIND CHARACTERISTICS

The study of the wind direction and velocity are important because these parameters can influence the rocket trajectory: 88% of trajectory corrections occur in the lower altitude, approximately 1000 m. Also, its knowledge is a key variable for the safety procedures during the rocket launching operations (Fisch 1999).

The predominant wind direction is from east, provoked by the trade winds and velocity it has a logarithmic profile with the altitude. The values vary between 6 m/s (typically during the wet season) to 10 m/s (during the dry period) (Fisch 1999; Gisler *et al.* 2011).

EXPERIMENTAL DESCRIPTION

The experiments were conducted in the aeronautic subsonic wind tunnel TA-2, located at the *Instituto de Aeronáutica e Espaço* (IAE), Brazil. The maximum mean velocity value through the wind tunnel test section is 120 m/s and the dimensions of the test section are 2.1 m vertical and 3.0 m lateral dimension.

ATMOSPHERIC BOUNDARY LAYER SIMULATED IN WIND TUNNEL

As the TA-2 is an aeronautic tunnel, with a short boundary layer thickness, a procedure was used for increasing the boundary layer thickness and for simulating the atmospheric boundary layer that typically occurs in ALC. Although flow characteristic in ALC would be more appropriately simulated in a boundary layer wind tunnel, the TA-2 wind tunnel is suitable, since the main purpose of this research is to make a comparative analysis considering different configuration of the coastal cliff and wind incidence angle in ALC.

In order to increase the turbulence within the tunnel it was used an arrangement of artificial devices as spires for simulating the vorticity; three slats of wood to give a better adjust for the flow; a barrier and wooden blocks to simulate the surface roughness, placed on the entrance of test section (Fig. 4a).

The size of the spires and the quantity of wooden blocks depend on the height of the boundary layer and the test section dimensions. The characteristic of these elements was estimated based on the work of Blessmann (1973). The velocity profile of ABL simulation was verified using two rakes of Pitot tubes in the middle of test section (Fig. 4b); more details of the procedure used can be seen in Faria (2016).

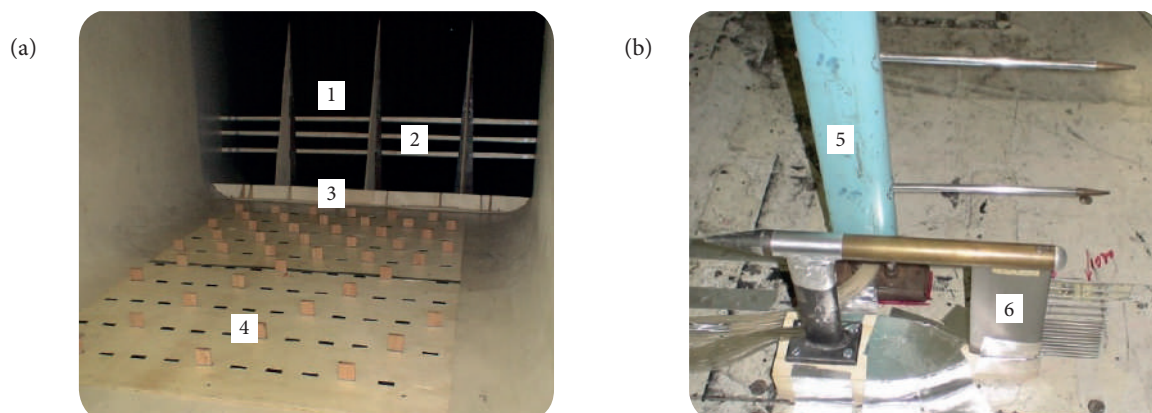


Figure 4. (a) Artificial devices for boundary layer atmospheric simulation – [1] Spires, [2] 3 Slats of wood, [3] Barrier and, [4] Wooden blocks; (b) Rakes of Pitot tubes – [5] Rake 1, and [6] Rake 2.

Many configurations with the artificial devices were tested for obtaining an appropriated wind velocity profile in the test section given by the Power Law equation (Eq. 1),

$$\frac{U(Z_r)}{U(Z_{ref})} = \left(\frac{Z_r}{Z_{ref}} \right)^\gamma \quad (1)$$

where $U(Z_{ref})$ is the mean velocity correspondent to a reference height Z_{ref} – the value is 10 m, which is the height recommended by the World Meteorology Organization (WMO) to represent the horizontal wind measurements at the surface. $U(Z_r)$, is the mean velocity correspondent to a reference height Z_r – the value used was 40 m, which corresponds to the coastal cliff height. The exponent γ is characteristic of the type of terrain, and varies from 0.11 for smooth surface as lakes and the ocean to 0.34 for cities with a high concentration of constructions. In the current study, the value 0.11 was considered because the wind at ACL comes from the ocean (Hsu *et al.* 1994; Barbosa *et al.* 2002). The resulted velocity profiles for different freestream velocity values (U_∞) of 10 m/s, 20 m/s, 30 m/s and 40 m/s were presented in Fig. 5.

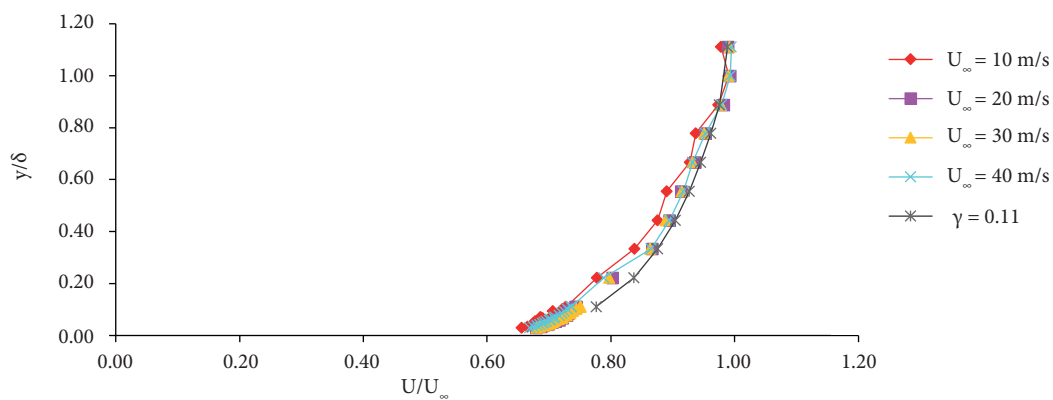


Figure 5. Velocity profiles obtain for different wind speeds.

TURBULENCE MEASUREMENTS

Once the wind profile was calibrated inside the wind tunnel, the turbulence measurements were conducted in the regions of interest in the wind tunnel test section, using a hot wire anemometer system and a manually controlled device positioned in the middle of test section (Fig. 6), which allowed the vertical displacement of the hot wire probe during the measurements. Because of a physical limitation of this device, the highest vertical position where turbulence measurements were conducted was 765 mm. For turbulence measurements, a straight golden-plated wire probe (55P01) was used and for data collection, a sample rate of 10 kHz was adopted. Turbulence measurements were performed for the freestream velocity of, approximately, 40 m/s and Reynolds number of 8.6×10^5 (Avelar *et al.* 2012).

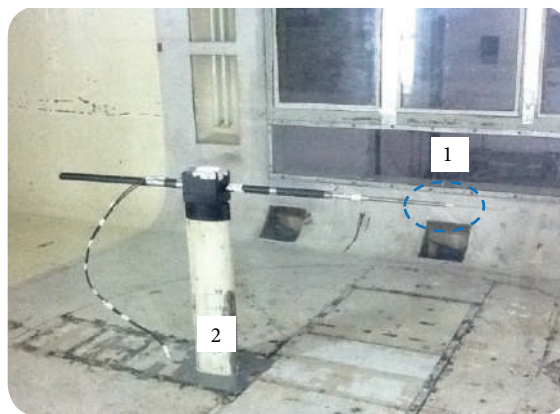


Figure 6. Hot wire probe in the middle of test section – (1) Hot wire probe; (2) Device.

The values of turbulence measurements are shown in Fig. 7. It can be seen a typical behavior of a wind tunnel flow when turbulence intensity is lower than 0.1 and they have higher values near the floor than at the middle of the test section, as expected. The work of Marciotto *et al.* (2012) presents some *in situ* data for atmospheric intensity, which vary between 0.13 and 0.26, higher than the measurements in the wind tunnel. This result is expected as the atmosphere is fully turbulent, and the wind tunnel is only its representation.

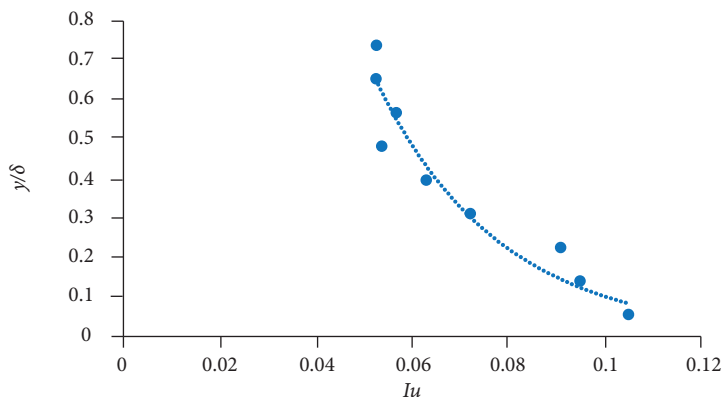


Figure 7. Velocity profile in the middle of test section.

PARTICLE IMAGE VELOCIMETRY MEASUREMENTS

Flow velocity measurements were carried out using a two-dimensional PIV system for investigating the flow near the MIT and launch vehicle. For this study, it was constructed a model of Launching Pad Area (LPA) (Fig. 8). This model was fixed over a wooden platform for simulating the coastal cliff inclination and painted in flat black to minimize the effects of laser reflections that can prejudice the quality of the experiments' results.

The wooden platform for simulating the coastal cliff inclination allowed the variation of coastal cliff inclination angle (β) and the wind incidence angle (α) in both top and frontal view of the wind tunnel model, which dimensions are shown in Fig. 9. In each tested configuration, the LPA model was rotated over a wooden platform for simulating the wind incidence and for simulating the coastal cliff slope angle (Fig. 9), wooden blocks were used in front of the wooden platform. For each value of α and β , the velocity values (U_∞) of 8 m/s, 20 m/s and 30 m/s, corresponding to Reynolds number (Re) of 1.7×10^5 , 4.3×10^5 and 6.4×10^5 , were considered.



Figure 8. LPA model.

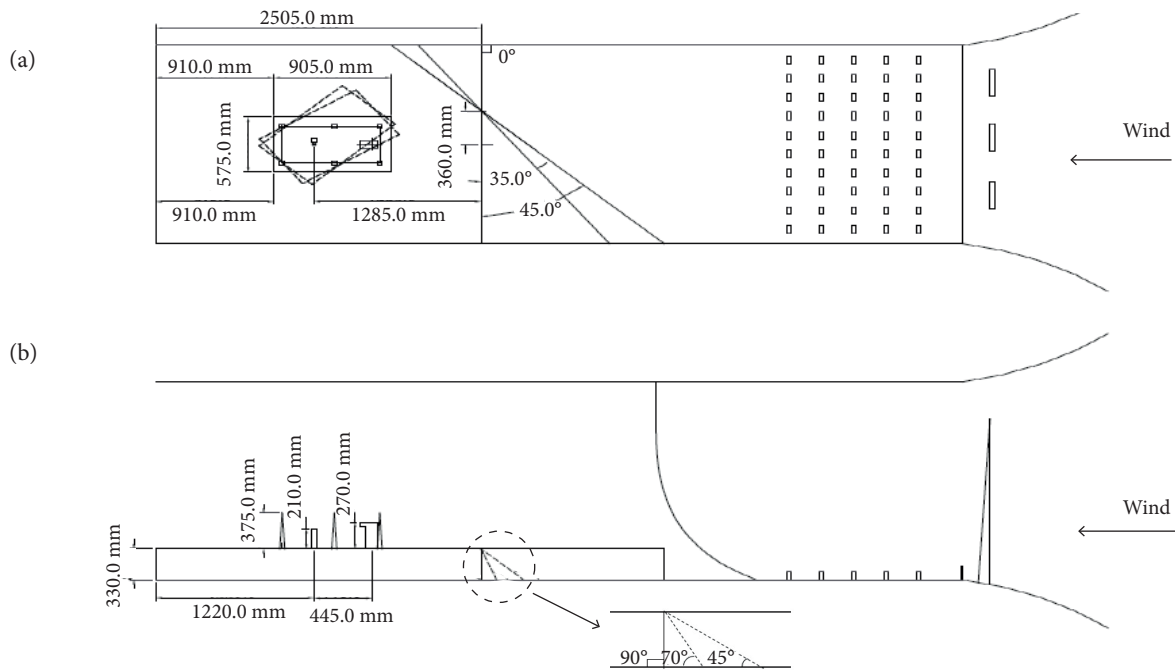


Figure 9. (a) Top view of the simulation of the wind incidence (α);
(b) Frontal view of the simulation of the coastal cliff inclination (β).

The mean velocity flow fields at the simulated Launch Pad Area (LPA) were obtained using a Dantec Dynamics two-dimensional PIV system. This system has a double-cavity pulsed laser, Nd:Yag, 15 Hz, with an output power of 200 mJ per pulse at the wave length of 532 nm (New Wave Research, Inc.) and two HiSense 4M CCD camera, built by Hamamatsu Photonics, Inc. with acquisition rate of 11 Hz, spatial resolution of 2048×2048 pixels, and $7.4 \mu\text{m}$ pixel pitch. A Nikon f# 2.8 lenses with 105 mm of focal length was used. The laser sheet created was putted in vertical plane (Fig. 10a), and was putted in horizontal plane (Fig. 10b). The flow was seeded with theatrical fog (polyethylene glycol water-solution) generated by a Rosco Fog Generator placed inside the wind tunnel diffuser. The images were pre-processed for decreasing laser flare effects and processed using the adaptive correlation option using commercial software Dynamic Studio version 3.20, developed by Dantec Dynamics. The adaptive correlation is a

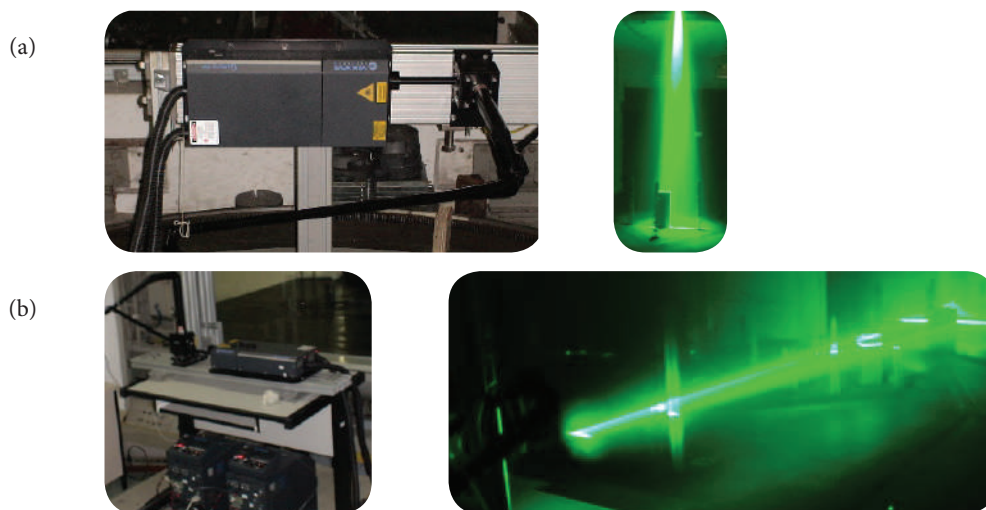


Figure 10. (a) PIV setup for measurements vertical plane; (b) PIV setup for measurements in horizontal plane.

cross correlation method used for estimating the spatial displacement between a pair of particles in an interrogation window. The images were processed using a 32×32 pixels interrogation windows with 50% overlap and moving average validation. The data were exported and analyzed using the software TECPLOT; for more details see Faria (2016).

Horizontal velocity fields were measured in three positions, 77 mm (name as P1 and P6), 155 mm (P2 and P5), and 255 mm (P3 and P4), corresponding to the aspect ratio, y/L , equal to 0.29, 0.68 and 0.94, respectively, being y the vertical positions of the laser and L the height of MIT model (270 mm). The laser light sheet was formed in a way to allow velocity field measurements in the wake of MIT as well as of the launch vehicle. The horizontal position of laser light sheet is indicated in Fig. 11.

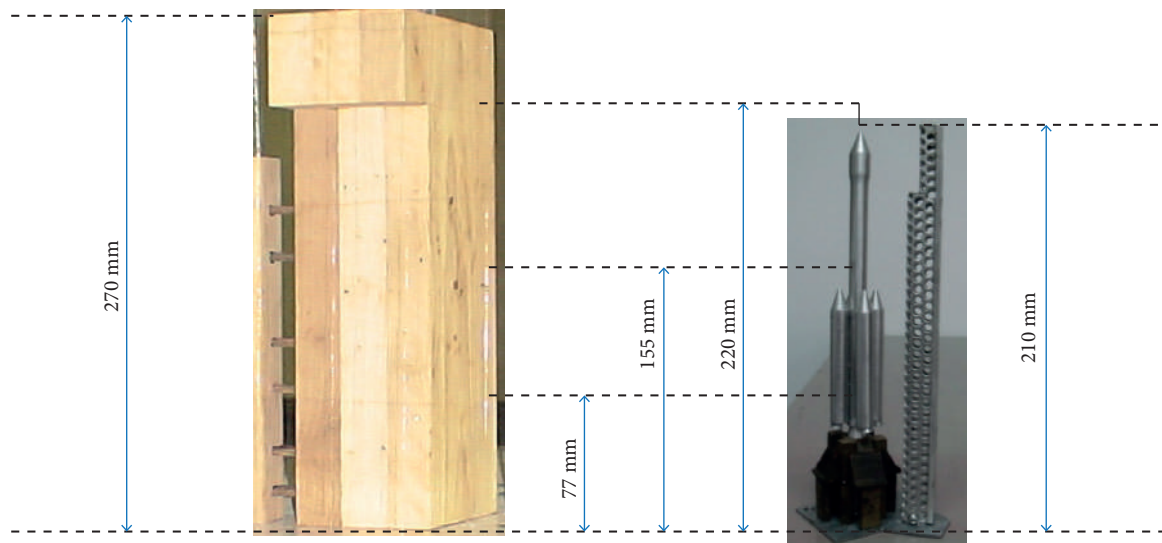


Figure 11. Heights of the horizontal plane of laser related to the heights of the MIT and launch vehicle.

RESULTS AND DISCUSSIONS

In order to investigate the flow patterns in the MIT region and launch vehicle region, experiments were carried out varying the following configurations: wind incidence directions (α), coastal cliff irregular structure (β) and variation of velocity the flow (U_∞) 8 m/s, 20 m/s and 30 m/s, that correspond the Reynolds numbers 1.7×10^5 , 4.3×10^5 and 6.4×10^5 . In this section, some obtained results will be presented and discussed.

VERTICAL PLANE IN THE REGION NEAR MIT

Figures 12, 13 and 14 show vorticity contours and velocity vectors maps in vertical planes in the neighborhood of MIT and on the entrance of coastal cliff, with $Re = 4.3 \times 10^5$, $\beta = 90^\circ$ and different wind incidence angles, α , 0° , 35° and 45° .

In Fig. 12b, when $\alpha = 0^\circ$ and $\beta = 90^\circ$, it can be observed the flow separation in the entrance of the coastal cliff and the creation of a recirculation bubble. The wind incidence in this case is $\alpha = 0^\circ$, which corresponds to a perpendicular position in relation to the flow in the wind tunnel test section and shoreline. No recirculation bubble is seen behind the MIT in this configuration (Fig. 12a).

In the flow maps shown in Figs. 13a and 14a, recirculation regions appears behind the MIT but not in the entrance of the coastal cliff. However, in Figs. 13b and 14b, the flow detaches in the border of MIT model and then separates again. These characteristics are related to the wind incidence angles.

It can be seen that the flow over the surface of the model separates more quickly in the conditions shown in Figs. 13a and 14a when compared with $\alpha = 0^\circ$ (Fig. 12a). The intensity in the recirculation region seems higher when $\alpha = 45^\circ$ (Fig. 14a) than when $\alpha = 35^\circ$ (Fig. 13a). This seems to happen because the model is rotated over the structure of the coastal cliff and the wind incidence

is more intense on the MIT structure. The lightning rod towers (Fig. 12) create shadows, despite of being out of the laser plane, which introduce difficulties to calculate the value of the velocity in this region.

It can be noted from the vorticity contours in Figs. 12, 13 and 14, that the mean vorticity values are in the range of -100 s^{-1} until 300 s^{-1} , the maximum vorticity value is 1000 s^{-1} and the minimum is -200 s^{-1} . It can be observed as well higher vorticity values at the border of MIT and at the entrance of coastal cliff. The vorticity values in this region are between the 700 s^{-1} and 1000 s^{-1} .

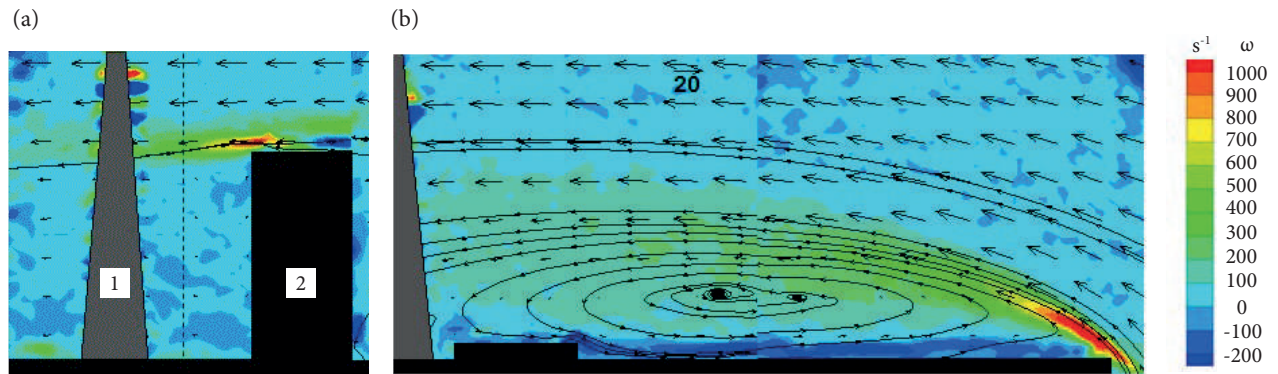


Figure 12. Vorticity contours and velocity vectors – $\beta = 90^\circ$, $\alpha = 0^\circ$ and $Re = 4.3 \times 10^5$. (a) Neighborhood MIT – (1) Lightning rod tower and (2) MIT; (b) Entrance of coastal cliff.

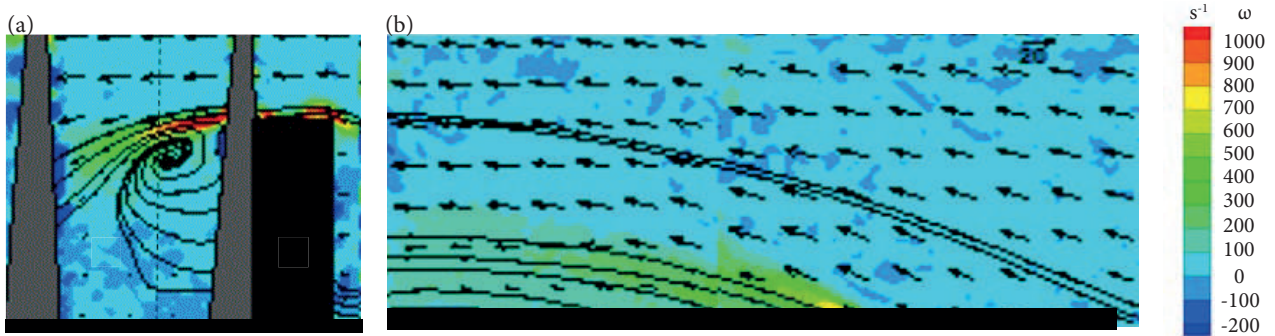


Figure 13. Vorticity contours and velocity vectors – $\beta = 90^\circ$, $\alpha = 35^\circ$ and $Re = 4.3 \times 10^5$. (a) Neighborhood MIT; (b) Entrance of coastal cliff.

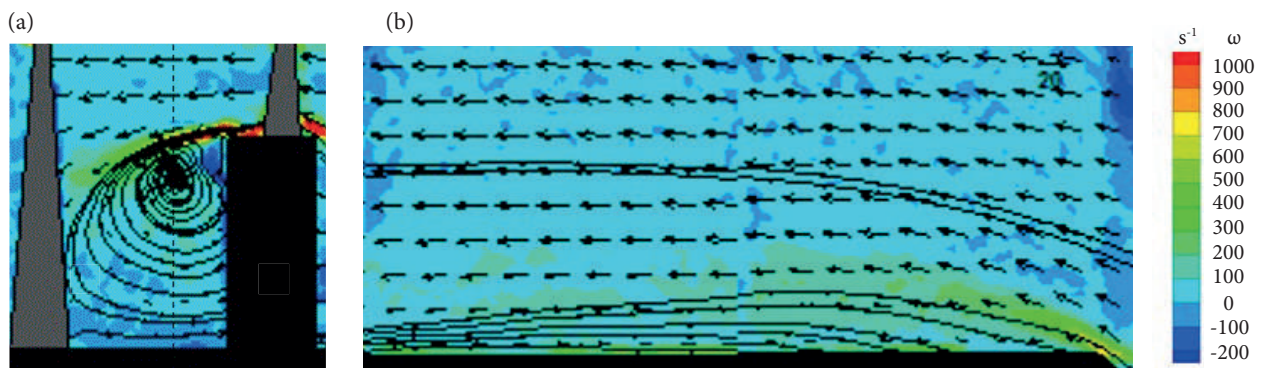


Figure 14. Vorticity contours and velocity vectors – $\beta = 90^\circ$, $\alpha = 45^\circ$ and $Re = 4.3 \times 10^5$. (a) Neighborhood MIT; (b) Entrance of coastal cliff.

Figure 15 shows the velocity profiles tracer in the MIT region, for $\beta = 90^\circ$ and $\alpha = 0^\circ$, $\alpha = 35^\circ$ and $\alpha = 45^\circ$ with $Re = 4.3 \times 10^5$. The black dashed lines in the Figs. 12, 13 and 14 indicate the region where the velocity profiles were extracted. As expected, for all values of α considered, $\alpha = 0^\circ$, $\alpha = 35^\circ$ and $\alpha = 45^\circ$, a flow deceleration aspect is observed behind the MIT.

For $\alpha = 35^\circ$ and $\alpha = 45^\circ$, negative velocity values behind the MIT can be observed due to recirculation regions formation, which seems not to occur for $\alpha = 0^\circ$. On the top of the MIT, the mean flow velocity is practically constant tending to the freestream condition. When $\alpha = 35^\circ$, the velocity flow is higher than the other two wind incidence angles $\alpha = 0^\circ$ and $\alpha = 45^\circ$.

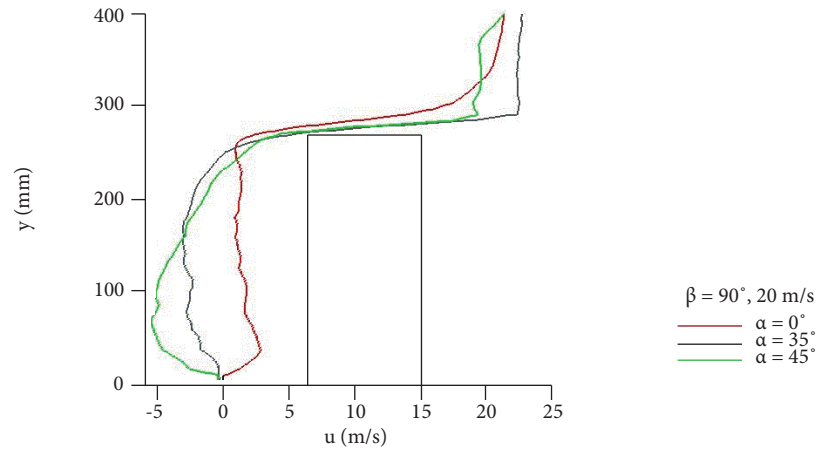


Figure 15. Velocity profiles in the MIT region for $\beta = 90^\circ$.

Figure 16 shows vorticity maps and velocity profiles extracted from flow maps in vertical plane with $Re = 4.3 \times 10^5$, $\beta = 70^\circ$ and wind incidences angles, α , of 0° , 35° and 45° .

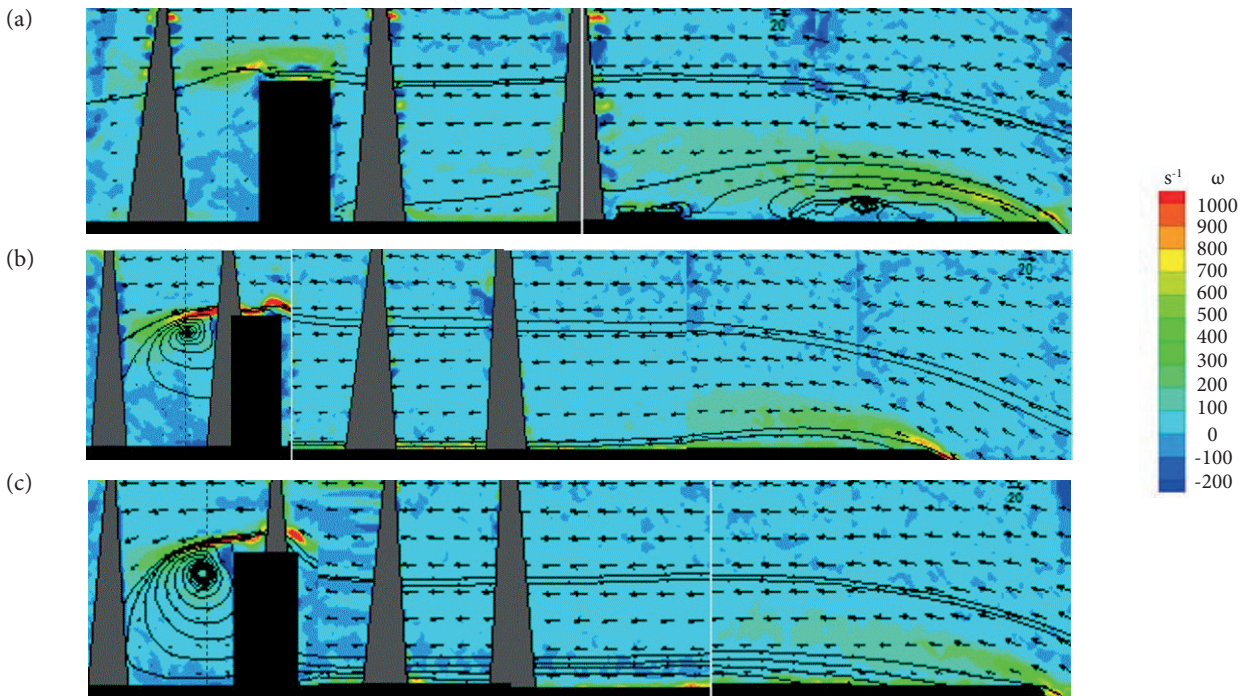


Figure 16. Vorticity contours and velocity vectors – $\beta = 70^\circ$, $Re = 4.3 \times 10^5$. (a) $\alpha = 0^\circ$; (b) $\alpha = 35^\circ$; (c) $\alpha = 45^\circ$.

In Fig. 16a, for $\alpha = 0^\circ$ and $\beta = 70^\circ$, it was observed the formation of a recirculation bubble on the entrance of coastal cliff that seems weaker than the one noted for $\alpha = 0^\circ$ and $\beta = 90^\circ$. This occurs because for $\beta = 70^\circ$ the entrance of the coastal cliff is less steep than for $\beta = 90^\circ$. In this case, no recirculation bubble is seen behind the MIT, but a big region of attached flow over the surface of the model is observed.

Figures 16b and 16c show a recirculation region behind the MIT but not on the entrance of the coastal cliff. The flow detaches on the border of the MIT model and separates behind it. It is observed that the flow over the model surface detaches faster in these two cases, when compared with $\alpha = 0^\circ$ (Fig. 16a). The recirculation region seems stronger when $\alpha = 45^\circ$ in comparison to $\alpha = 35^\circ$, as observed in Figs. 14a and 13a.

It can be seen, from the vorticity fields (Fig. 16), that the mean vorticity values are in the range of -100 s^{-1} until 300 s^{-1} , the maximum vorticity value is 1000 s^{-1} and the minimum is -200 s^{-1} . It can be observed an intense vorticity near the border of MIT and on the entrance of the coastal cliff, because of the deceleration of flow near these regions. The vorticity values in these areas are between 700 s^{-1} and 1000 s^{-1} . The velocity profiles in the MIT region, for $\beta = 70^\circ$, in general, is similar to the velocity profiles for $\beta = 90^\circ$.

The flow maps in Figs. 17a, 18a and 19a show a recirculation region behind the MIT and not on the entrance of coastal cliff. This happens because when the cliff is inclined of $\beta = 45^\circ$, the entrance of coastal cliff is less stiff than for $\beta = 90^\circ$ and $\beta = 70^\circ$, and the wind detaches on the border of MIT building.

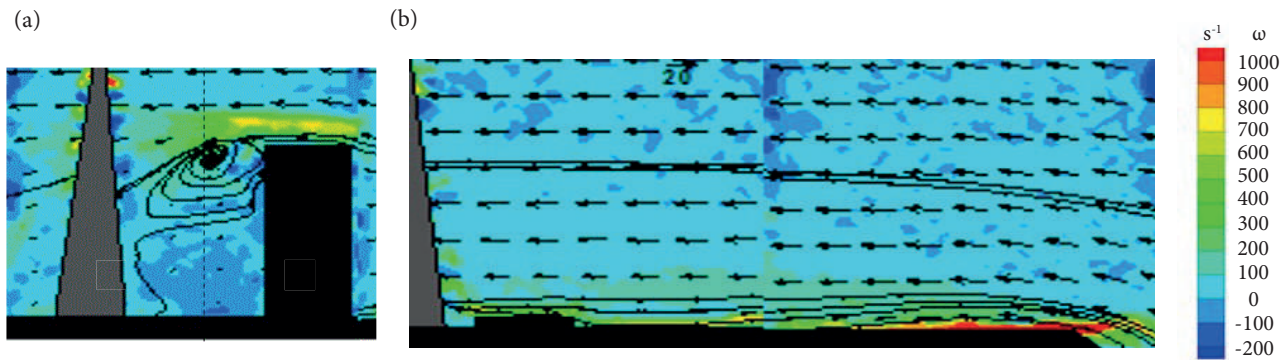


Figure 17. Vorticity contours and velocity vectors – $\beta = 45^\circ$, $\alpha = 0^\circ$ and $Re = 4.3 \times 10^5$.
(a) Neighborhood MIT; (b) Entrance of coastal cliff.

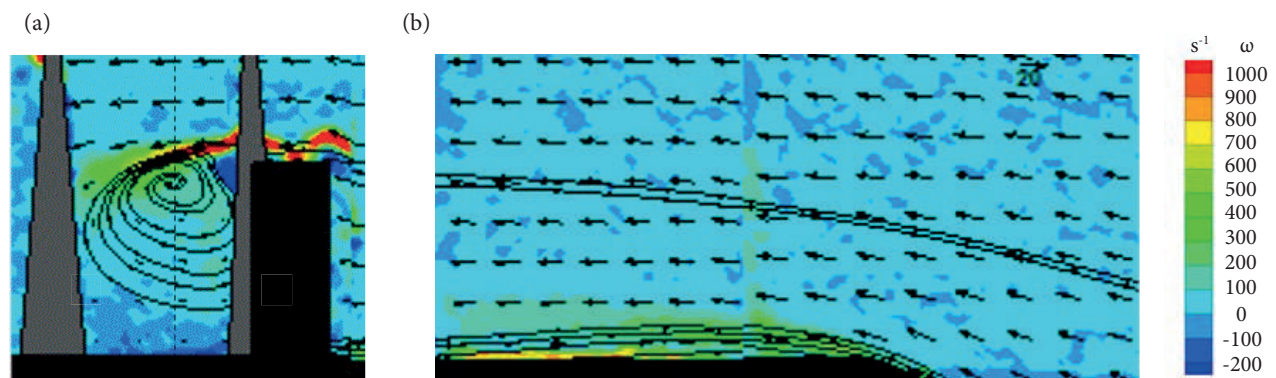


Figure 18. Vorticity contours and velocity vectors – $\beta = 45^\circ$, $\alpha = 35^\circ$ and $Re = 4.3 \times 10^5$.
(a) Neighborhood MIT; (b) Entrance of coastal cliff.

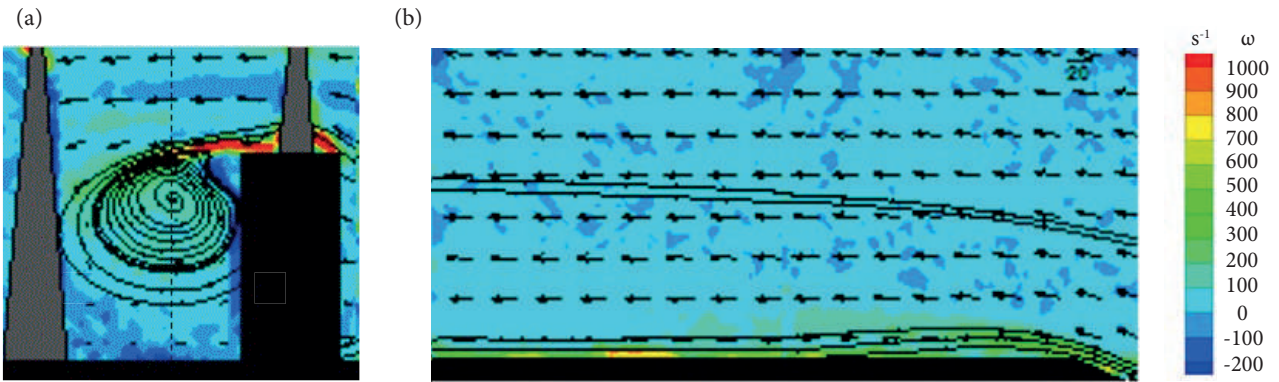


Figure 19. Vorticity contours and velocity vectors – $\beta = 45^\circ$, $\alpha = 45^\circ$ and $Re = 4.3 \times 10^5$.
 (a) Neighborhood MIT; (b) Entrance of coastal cliff.

It can be seen in the vorticity scale in Figs. 17, 18 and 19 that most of the vorticity values is concentrate in the range -100 s^{-1} until 300 s^{-1} , the maximum vorticity is 1000 s^{-1} and the minimum is -200 s^{-1} . It can be seen an intense vorticity near the border of MIT and on the entrance of coastal cliff, this occurs because of the deceleration the flow near these locals. The vorticity values in these locals are between 700 s^{-1} and 1000 s^{-1} .

Figure 20 shows the velocity profiles near the MIT region for $\beta = 45^\circ$ and $\alpha = 0^\circ$, $\alpha = 35^\circ$ and $\alpha = 45^\circ$ with $Re = 4.3 \times 10^5$. One more aspect to be observed is that the velocity profile for $\alpha = 45^\circ$ seems to take more time to attain the free stream condition, which can be a consequence of a wake with a more intense recirculation region since the velocity profile was extracted in a line passing through the recirculation bubble. On the top of the MIT the velocity is practically constant. When $\alpha = 35^\circ$ the velocity value is higher than the other two wind incidence angles $\alpha = 0^\circ$ and $\alpha = 45^\circ$.

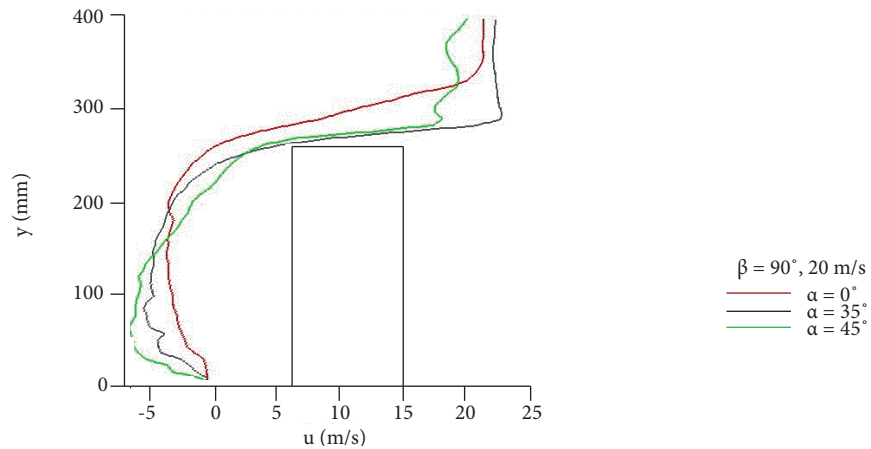


Figure 20. Velocity profiles in the MIT region for $\beta = 45^\circ$.

Table 1 shows a summary of the flow pattern characteristics when the measurements were carried out in vertical planes.

Figure 21 shows the vorticity maps and velocity vectors for $\beta = 45^\circ$ and $\alpha = 45^\circ$, when the Reynolds number were varied. It can be observed that the position over the model surface where the flow detaches do not change with the Re number variation. When Re increases, a more intense vorticity field can be noted on the border of the MIT, as well as a small region over the MIT of attached flow. The intensity of the recirculation region in the three cases shown in Fig. 21 is similar.

In Fig. 21 it can be observed that the flow separation occurs always on the same position, over the MIT and on the border of the model, as expected, since, the Re number does not influence the flow pattern in separated flows (Loredo-Souza *et al.* 2004).

Table 1. Flow pattern characteristics in vertical planes of measurements in the MIT neighborhood.

Vertical planes of measurements				
Re number	Configurations		Separation of flow on the entrance of coastal cliff	Recirculation region near the MIT
4.3×10^5	$\beta = 90^\circ$	$\alpha = 0^\circ$	Yes	No
		$\alpha = 35^\circ$	No	Yes
		$\alpha = 45^\circ$	No	Yes
	$\beta = 45^\circ$	$\alpha = 0^\circ$	No	Yes
		$\alpha = 35^\circ$	No	Yes
		$\alpha = 45^\circ$	No	Yes
	$\beta = 70^\circ$	$\alpha = 0^\circ$	Yes	No
		$\alpha = 35^\circ$	No	Yes
		$\alpha = 45^\circ$	No	Yes

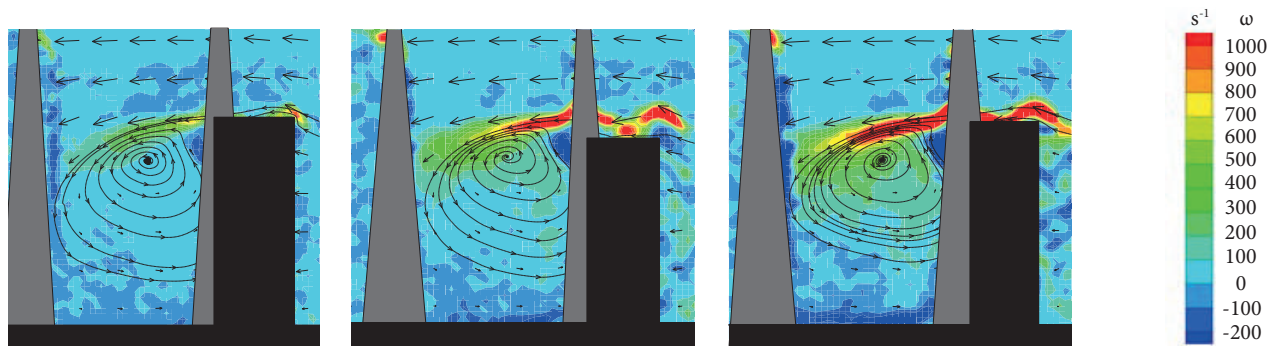


Figure 21. Vorticity contours and velocity vectors – $\beta = 45^\circ$ and $\alpha = 45^\circ$, and varying the Re number.

HORIZONTAL PLANE OF MEASUREMENTS IN THE LAUNCH VEHICLE NEIGHBORHOOD

Figures 22 to 25 show the vorticity maps and velocity vectors in horizontal planes of measurement. These configurations represent the flow characteristics of the Launch Pad Area (LPA) in the following height: $y/L = 0.29, 0.68$ and 0.96 , $\alpha = 35^\circ$ and 45° , $\beta = 45^\circ$, $\beta = 70^\circ$ and $\beta = 90^\circ$ and velocity value (U_∞) equal 8 m/s ($Re = 1.7 \times 10^5$).

The flow maps in Fig. 22 show the results of the lowest horizontal plane of measurement, $y/L = 0.29$, $\alpha = 45^\circ$ and $Re = 1.7 \times 10^5$. In Figs. 22a ($\beta = 45^\circ$) and 22c ($\beta = 70^\circ$) it can be observed the occurrence of two recirculation regions behind the exit tower. In Fig. 22b ($\beta = 90^\circ$) one recirculation region with disoriented vortexes can be observed. Also, the vorticity intensity is more intense near the border of exit tower and launch vehicle, and near the wires that connect the lightning rod towers. The mean vorticity values are in the range -200 s^{-1} until 200 s^{-1} .

The flow maps in Fig. 23 show the intermediate measurement plane, $y/L = 0.68$, $\alpha = 35^\circ$ and $Re = 1.7 \times 10^5$. In the Figs. 23a ($\beta = 45^\circ$) and 23c ($\beta = 70^\circ$) one recirculation region with disoriented vortexes is observed behind the exit tower. In Fig. 23b ($\beta = 90^\circ$) no recirculation region behind the exit tower is observed. Another observation is that the vorticity intensity is greater near the border of exit tower and launch vehicle and near the wires that of connect the lightning rod towers, as observed in Fig. 22. The mean vorticity values are in the range -200 s^{-1} until 200 s^{-1} .

The flow maps in Fig. 24 show the results for $y/L = 0.96$, $\alpha = 45^\circ$, varying the Reynolds Number (1.7×10^5 , 4.3×10^5 and 6.4×10^5) and the coastal cliff slope inclination (β). In Fig. 24a ($\beta = 45^\circ$) one recirculation region is observed behind the exit tower. In Figs. 24b ($\beta = 90^\circ$) and 24c ($\beta = 90^\circ$) no recirculation region is observed behind this tower. Another observation is that the vorticity intensity is more intense near the border of exit tower and launch vehicle and around the wires that of connect the lightning rod towers, as observed in Figs. 22 and 23.

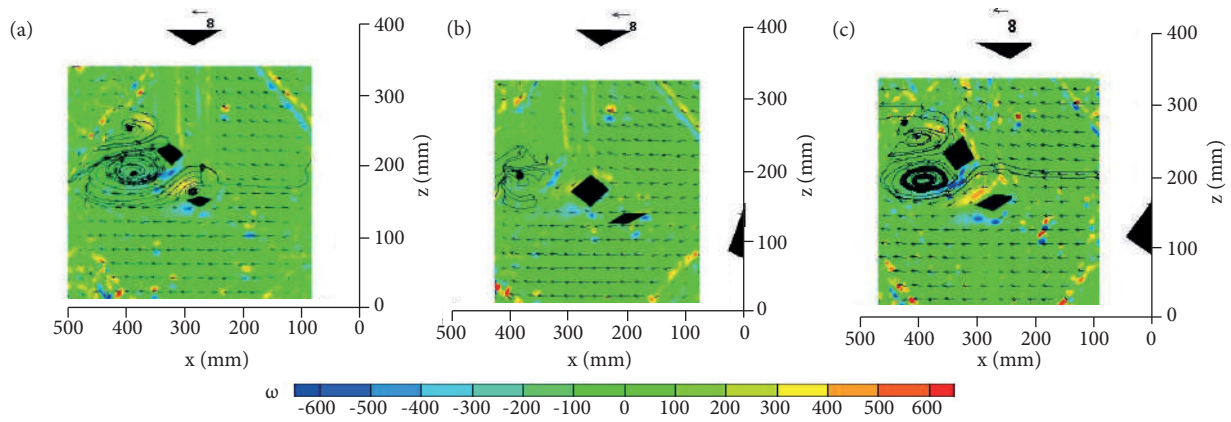


Figure 22. Vorticity contours and velocity vectors varying the inclination of coastal cliff for $y/L = 0.29$, $\alpha = 45^\circ$ and $Re = 1.7 \times 10^5$. (a) $\beta = 45^\circ$; (b) $\beta = 90^\circ$ - [1] Lightning rod towers, [2] Exit tower and [3] Launch vehicle and umbilical tower; (c) $\beta = 70^\circ$.

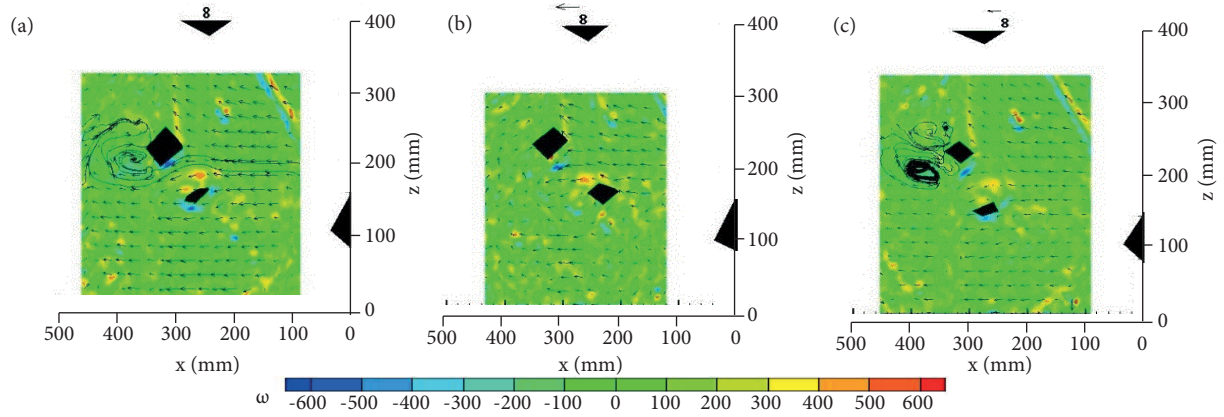


Figure 23. Vorticity contours and velocity vectors varying the coastal cliff inclination with $y/L = 0.68$, $\alpha = 35^\circ$ and $Re = 1.7 \times 10^5$. (a) $\beta = 45^\circ$; (b) $\beta = 90^\circ$; (c) $\beta = 70^\circ$.

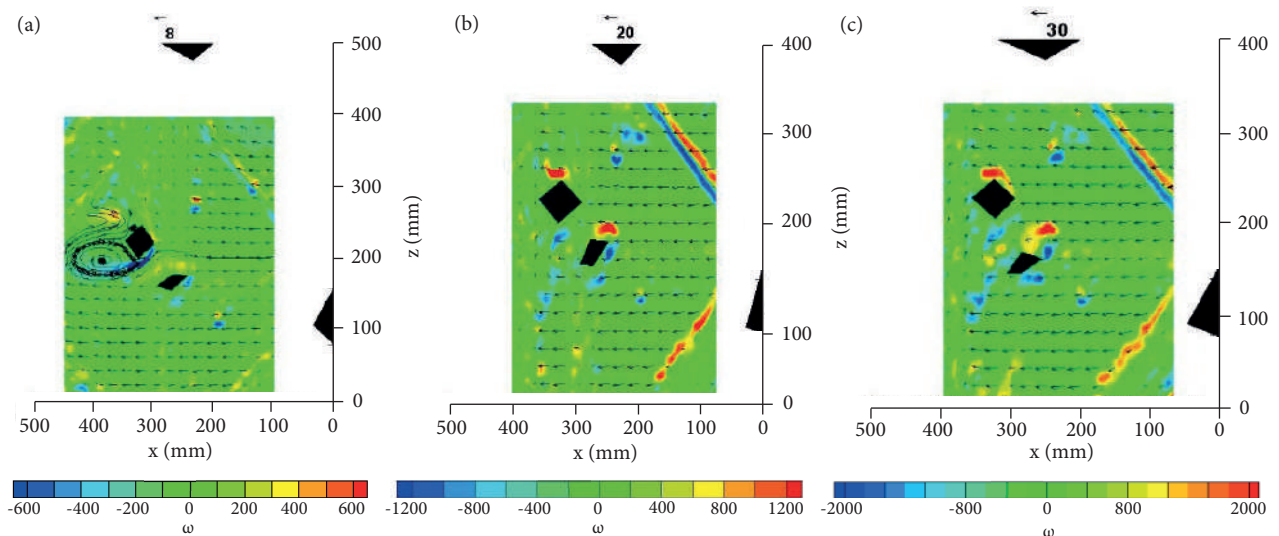


Figure 24. Vorticity contours and velocity vectors varying the coastal cliff inclination and the Re number with $y/L = 0.96$, $\alpha = 45^\circ$. (a) $\beta = 45^\circ$; (b) $\beta = 90^\circ$; (c) $\beta = 90^\circ$.

Table 2 shows a summary of the flow pattern characteristics when the measurements were carried out in horizontal planes.

Table 2. Flow pattern characteristics in horizontal planes of measurements in the launch vehicle neighborhood.

Horizontal planes of measurements						
y/L	Re number	Configurations		One recirculation region	Two recirculation region	No recirculation region
0.29	1.7×10^5	$\alpha = 35^\circ$	$\beta = 90^\circ$	No	Yes	-
			$\beta = 45^\circ$	No	Yes	-
			$\beta = 70^\circ$	No	Yes	-
	1.7×10^5	$\alpha = 45^\circ$	$\beta = 90^\circ$	Yes	No	-
			$\beta = 45^\circ$	No	Yes	-
			$\beta = 70^\circ$	No	Yes	-
	4.3×10^5	$\alpha = 45^\circ$	$\beta = 70^\circ$	No	Yes	-
6.4×10^5	$\alpha = 45^\circ$	$\beta = 70^\circ$	No	Yes	-	
4.3×10^5	$\alpha = 35^\circ$	$\beta = 90^\circ$	No	Yes	-	
0.68	1.7×10^5	$\alpha = 35^\circ$	$\beta = 90^\circ$	No	No	Yes
			$\beta = 45^\circ$	Yes	No	-
			$\beta = 70^\circ$	No	Yes	-
	1.7×10^5	$\alpha = 45^\circ$	$\beta = 90^\circ$	No	No	Yes
			$\beta = 45^\circ$	Yes	No	-
			$\beta = 70^\circ$	Yes	No	-
	4.3×10^5	$\alpha = 35^\circ$	$\beta = 90^\circ$	Yes	No	-
6.4×10^5	$\alpha = 45^\circ$	$\beta = 70^\circ$	Yes	No	-	
0.96	1.7×10^5	$\alpha = 35^\circ$	$\beta = 45^\circ$	No	No	Yes
	4.3×10^5		$\beta = 70^\circ$	No	No	Yes
	6.4×10^5		$\beta = 90^\circ$	No	No	Yes
	1.7×10^5	$\alpha = 45^\circ$	$\beta = 45^\circ$	Yes	No	-
	4.3×10^5		$\beta = 90^\circ$	No	No	Yes
	6.4×10^5		$\beta = 90^\circ$	No	No	Yes

The flow maps in Fig. 25 show a comparison in horizontal planes of measurements considering $\beta = 90^\circ$, $\alpha = 45^\circ$ and $Re = 1.7 \times 10^5$. When $y/L = 0.29$ (Fig. 25a), one recirculation region can be observed behind the exit tower. For $y/L = 0.68$ (Fig. 25b) and $y/L = 0.96$ (Fig. 25c), some disoriented vortexes is noted behind exit tower.

These different aspects in the flow behind the exit tower occur because the vortex regions suffer influences of the boundary layer when $y/L = 0.29$. For the other heights ($y/L = 0.68$ and 0.96) the velocity behind the exit tower increases and become close to the freestream velocity values in wind tunnel test section. The mean vorticity values are in the range -100 s^{-1} until 200 s^{-1} .

ATMOSPHERIC DISPERSION OF PROPELLANTS NEIGHBORHOOD THE MIT

The wind is the meteorology component associated with the atmospheric dispersion of propellants. The lower wind velocities allow more concentration of propellants near Launch Pad Area (LPA). Because of this, the velocity of 8 m/s was chosen for this study.

The turbulence intensity maps are show in Fig. 26. It was calculated from horizontal fields of standard deviation and flow velocity (U_∞). It can be observed in the neighborhood MIT that the turbulence intensity is weaker when compared with other regions of the flow, because of the recirculation bubble present in this region. In Fig. 26a ($y/L = 0.29$) the flow seems more disturbed because of the laser position to be close of the floor and the turbulence intensity seems higher due to the friction with the surface.

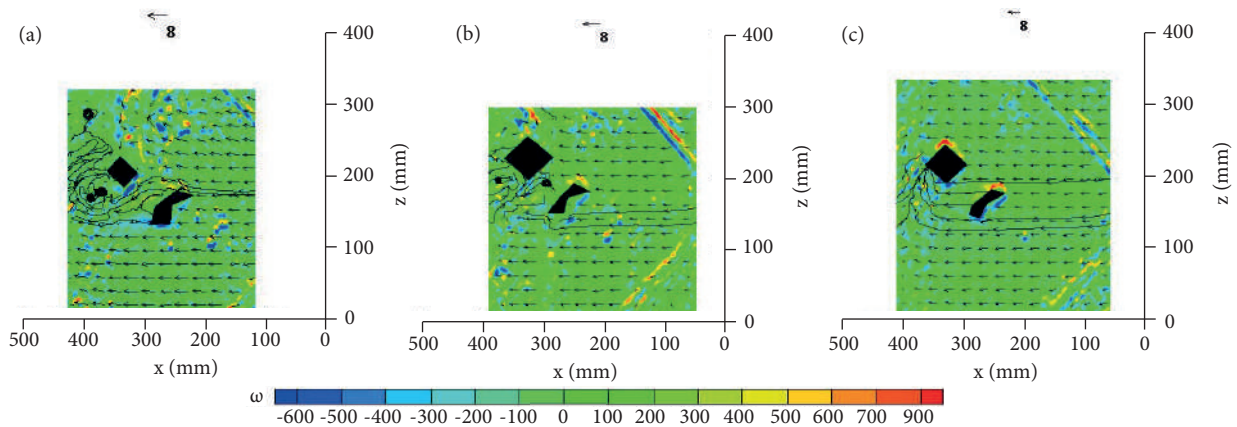


Figure 25. Vorticity contours and velocity vectors varying the height of laser plane for $\alpha = 45^\circ$, $\beta = 90^\circ$ and $Re = 1.7 \times 10^5$. (a) $y/L = 0.29$; (b) $y/L = 0.68$; (c) $y/L = 0.96$.

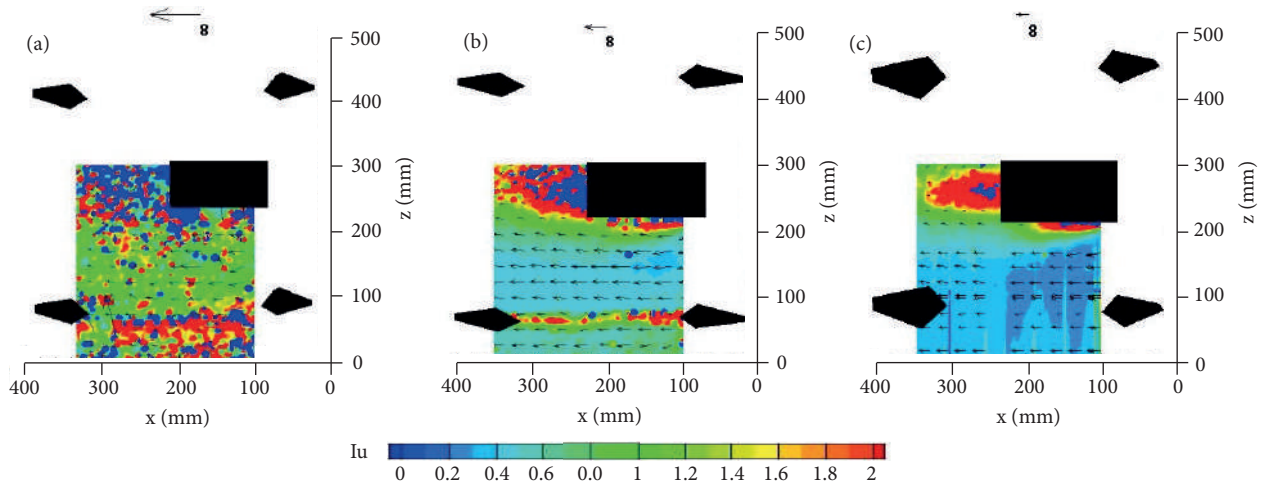


Figure 26. Turbulence Intensity and velocity vectors for $\alpha = 0^\circ$, $\beta = 90^\circ$, $Re = 1.7 \times 10^5$ and varying the height of laser plane. (a) $y/L = 0.29$; (b) $y/L = 0.68$; (c) $y/L = 0.96$.

In Figs. 26b ($y/L = 0.68$) and 26c ($y/L = 0.96$) the turbulence intensity values are in the range 0.2 and 0.4. These values are higher than the values observed in ACL region (Marciotto *et al.* 2012).

CONCLUSIONS

Based on the investigation carried out and the results presented, the following conclusions can be pointed out:

- The regions with recirculation due to the presence of MIT were identified in both horizontal and vertical planes using PIV techniques, which was expected since the flow investigated is highly tridimensional;
- For the horizontal plane, it was observed that the different configurations of wind incidence and coastal cliff inclinations analyzed changed the flow pattern near the exit tower. Once two recirculation regions appeared, one is more intense than the other;
- For the vertical planes the separation position of the flow do not change with Re numbers variation and presents a typical behavior of the separated flow. Also, the recirculation region behind the MIT is more intense when $\alpha = 45^\circ$ and when $\alpha = 35^\circ$, being the vortex more defined. For the $\alpha = 0^\circ$ and $\beta = 70^\circ$ and $\beta = 90^\circ$, there is no recirculation vortex developed;

- The vortexes pattern behind the MIT or exit tower structures is strongly influenced by the wind incidence angles. These vortexes may induce vibrations or load excess on these buildings structures if they remain there for a long time.

In general, changes in configurations of wind incidence angles and the presence of the coastal cliff inclination can modify the flow patterns near de Launching Pad Area (LPA). This fact can affect the safety during the rocket launching, because of its possible influence in the rocket trajectory and the dispersion of gases released by burning propellants. These are some scientific contributions, of this work for the Brazilian Space Program.

AUTHOR'S CONTRIBUTION

Conceptualization, Avelar AC and Fisch G; Methodology, Avelar AC and Faria AF; Investigation, Avelar AC, Faria AF and Fisch G; Writing, Avelar AC, Faria AF and Fisch G; Funding Acquisition, Avelar AC and Fisch G; Resources, Avelar AC and Fisch G; Supervision, Avelar AC and Fisch G.

FUNDING

<http://dx.doi.org/10.13039/501100003593> - Conselho Nacional de Desenvolvimento Científico e Tecnológico

Grant No: 403899/2016-8

<http://dx.doi.org/10.13039/501100002322> - Coordenação de Aperfeiçoamento de Pessoal de Nível Superior

Grant Nos: Pró-Estratégia 2240/2012; DT 308829/2015-8; PQ 308011/2014-7

REFERENCES

Avelar AC, Brasileiro FLC, Marto AG, Marciotto ER, Fisch G, Faria AL (2012) Wind tunnel simulation of the atmospheric boundary layer for studying the Wind pattern at *Centro de Lançamento de Alcântara*. *Journal of Aerospace Technology and Management* 4(4):463-473. <https://doi.org/10.5028/jatm.2012.04044912>

Avelar AC, Fisch G, Faria AF, Brasileiro FLC (2014) Wind tunnel study of wind flow patterns in the Alcântara Space Launching Center. Presented at: 44th AIAA Fluid Dynamics Conference; Atlanta, USA. <https://doi.org/10.2514/6.2014-3326>

Barbosa PHA, Cataldi M, Freire APS (2002) Wind tunnel simulation of atmospheric boundary layer flows. *Journal of the Brazilian Society of Mechanical Sciences* 24(3):177-185. <https://doi.org/10.1590/S0100-73862002000300005>

Baskaran A, Kashef A (1996) Investigation of air flow around buildings using computational fluid dynamics techniques. *Engineering Structures* 18(11):861-875. [https://doi.org/10.1016/0141-0296\(95\)00154-9](https://doi.org/10.1016/0141-0296(95)00154-9)

Blessmann J (1973) Simulação da estrutura do vento natural em um túnel de vento aerodinâmico (PhD Thesis). São José dos Campos: Instituto Tecnológico da Aeronáutica. In Portuguese.

Caruzzo A, Belderrain MCN, Fisch G, Manso DF (2015) The mapping of aerospace meteorology in the Brazilian Space Program: challenges and opportunities for rocket launch. *Journal of Aerospace Technology and Management* 7(1):7-18. <https://doi.org/10.5028/jatm.v7i1.461>

Faria AF (2016) Análise experimental do escoamento atmosférico no Centro de Lançamentos de Alcântara utilizando túnel de vento (Master's Dissertation). São José dos Campos: Instituto Tecnológico de Aeronáutica. In Portuguese.

Fisch G (1999) Características do perfil vertical do vento no Centro de Lançamento de Foguetes de Alcântara (CLA). *Revista Brasileira de Meteorologia* 14(1):11-21.

Fox RW, Pritchard JP, McDonald AT (2014) *Introdução à mecânica dos fluidos*. 8th ed. Rio de Janeiro: LTC.

Garratt JR (1992) *The atmospheric boundary layer*. Cambridge: Cambridge University Press.

- Gisler CAF, Fisch G, Correa CS (2011) Análise estatística do perfil de vento na camada limite superficial no Centro de Lançamento de Alcântara. *Journal of Aerospace Technology and Management* 3(2):193-202. <https://doi.org/10.5028/jatm.2011.03022411>
- Griffin OM (1985) Vortex shedding from bluff bodies in a shear flow: a review. *Journal of Fluids Engineering* 107(3):298-306. <https://doi.org/10.1115/1.3242481>
- Hsu SA, Meindl EA, Gilhousen DB (1994) Determining the power-law wind-profile exponent under near-neutral stability conditions at sea. *Journal of Applied Meteorology* 33(6):757-765. [https://doi.org/10.1175/1520-0450\(1994\)033<0757:DTPLWP>2.0.CO;2](https://doi.org/10.1175/1520-0450(1994)033<0757:DTPLWP>2.0.CO;2)
- Loredo-Souza AC, Schettini EBC, Paluch MJ (2004) Simulação da camada limite atmosférica em túnel de vento. Presented at: Escola de Primavera de Transição e Turbulência; Porto Alegre, Brazil.
- Marciotto ER, Fisch G, Medeiros LE (2012) Characterization of surface level Wind in the Centro de Lançamento de Alcântara for use in rocket structure loading and dispersion studies. *Journal of Aerospace Technology and Management* 4(1):69-79. <https://doi.org/10.5028/jatm.2012.04014911>
- Meneghini, J. R. Ássi GRS, Orselli RM, Carmo BS, Saltara F, Gioria RS, Bonatto A, Tsiloufas S (2010) Ruído e vibração induzidos por vórtices. Presented at: Escola de Primavera de Transição e Turbulência; Ilha Solteira, Brazil.
- Pires LBM (2009) Estudo da camada limite interna desenvolvida em falésias com aplicação para o Centro de Lançamento de Alcântara (PhD Thesis). São José dos Campos: Instituto Nacional de Pesquisas Espaciais. In Portuguese.
- Roballo ST (2007) Estudo do escoamento atmosférico no Centro de Lançamento de Alcântara (CLA) através de medidas de torre anemométrica e em túnel de vento (Master's Dissertation). São José dos Campos: Instituto Nacional de Pesquisas Espaciais. In Portuguese.
- Vatistas GH, Lin S, Kwok CK (1986) Reverse Flow Radius in Vortex Chambers. *AIAA Journal* 24(11):1872-1873. <https://doi.org/10.2514/3.9539>
- Vaughan WW, Johnson DL (2011) Aerospace meteorology: some lessons learned from the development and application of NASA terrestrial environment design criteria. *Bulletin of the American Meteorological Society* 92(9):1149-1157, 2011. <https://doi.org/10.1175/2011BAMS3133.1>
- Wittwer AR (2006) Simulação do vento atmosférico e dos processos de dispersão de poluentes em túnel de vento (PhD Thesis). Porto Alegre: Universidade Federal do Rio Grande do Sul. In Portuguese.
- Woo HGC, Peterka JA, Cemarm JE (1977) Wind tunnel measurements in the wakes of structures. (NASA-CR-2806). NASA Technical Report.